DFT study on zeolites' intrinsic Brønsted acidity: the case of BEA

Laura Gueci[a], Francesco Ferrante[a,*], Marco Bertini[a], Chiara Nania[a], Dario Duca[a]

[a]*Dipartimento di Fisica e Chimica "E. Segrè" - Università degli Studi di Palermo, Viale delle Scienze Ed. 17, I-90128 Palermo, Italy*

Abstract

Since Brønsted acidity is a crucial aspect for the applications of zeolitic materials in heterogeneous catalysis, great effort was devolved to characterize the number, strength and location of the potentially active acidic sites. Quantum chemical calculations can turn out essential in estimating the intrinsic acidity by computing deprotonation energy (DPE) values, although each method comes with its own difficulties. In this context, three approaches within density functional theory were employed to study the intrinsic acidity of 30 topologically distinct Brønsted sites in the β-zeolite framework. Advantages and disadvantages of the three methods were outlined and the acidity order between the sites was assessed, being the DPE range 59 kJ mol^{-1} wide, with the proposed best approach. By dividing the range into three portions, the sites were classified as having high, medium and low acidity. Hydrogen bonds formation was found to be a contributing factor in determining a low Brønsted acidity.

Keywords: β-zeolite, DFT, intrinsic acidity, topological sites

1. Introduction

Zeolites are crystalline aluminosilicates with a specific microporous structure that find wide application as heterogeneous catalysts, especially in the petrochemical industry [1–6]. From the isomorphous substitution of a silicon atom by an aluminum atom in the

*Corresponding author

Email addresses: `laura.gueci@unipa.it` (Laura Gueci), `francesco.ferrante@unipa.it` (Francesco Ferrante), `marco.bertini@unipa.it` (Marco Bertini), `chiara.nania@unipa.it` (Chiara Nania), `dario.duca@unipa.it` (Dario Duca)

pure-silica framework, a negative charge is generated which can be balanced by a proton. This gives rise to the zeolites' pronounced Brønsted acidic properties, responsible for most of their usage and notability [7–9]. The intrinsic strength of a zeolite Brønsted acidic site can be quantified in terms of its deprotonation energy (DPE), that is the energy needed to separate a proton at an infinite distance from the resulting anion. In real systems, however, Brønsted acidity can only be observed if a base is present, so that additional factors become important, such as accessibility of the involved zeolitic site, steric hindrance, the tendency of the base to accept protons, and the stabilization of the resulting ion pair.

According to this distinction, large effort was devoted, both through theoretical studies and experimental tecniques, to characterize the number, strength, and location of the potentially active acidic sites, aiming at a formulation of acidity-reactivity relationships in zeolite catalysis [10–13]. As a matter of fact, the synergism between experiment and quantum chemistry calculation is instrumental to unveil the fundamental aspects of catalytic reactions, assisting the design of new catalysts and orienting the optimization of active sites [14–21]. For zeolite-based catalyst specifically, Density Functional Theory (DFT) proved to be essential in the development of materials and processes [22–25]. Common approaches to measure proton affinity of zeolites include IR and NMR spectroscopy, calorimetry and temperature-programmed desorption (TPD), exploiting the interaction of the acidic sites with basic probe molecules such as ammonia and pyridine [26–30]. Ammonia IRMS-TPD experiments, for example, have been successfully used in combination with DFT studies to assign the stretching vibration bands of acidic OH groups in the IR spectrum to each Brønsted acidic site, located at crystallographically non-equivalent position in MOR, FAU, CHA and BEA zeolite frameworks [31–34]. The Brønsted acidity of sites belonging to FAU, CHA, IFR, MOR, FER, and TON zeolites was investigated by Trachta *et al.* [35] by the analysis of the adsorption of base molecules with different proton affinities. Even if the authors recognize the difficulties in estimating a site acidity ranking, they recommended a best acidity order based on the use of probes (such as acetonitrile) whose proton affinity is just below the site deprotonation threshold. However, it is our opinion that the use of the adsorption properties of small molecules to sample the acidity of zeolites Brønsted sites is complicated by the orientation of the

probe with respect to the zeolite framework. As a matter of fact, this orientation is driven by a delicate balance between the directional interaction with the acid hydrogen atom and a number of weak interactions with the zeolite walls; just these latters, from the computational point of view, are very difficult to be estimated and, even if a number of correction schemes for dispersion interactions was proposed in the recent years, it is not guaranteed that these corrections allow to reach the accuracy needed for the most reliable description. Accordingly, it is perhaps a better idea to avoid these complications and resort to acidity rankings based on deprotonation energies, even if this quantity is not accessible by direct measurements [36].

DPEs in various zeolites have been estimated from quantum chemical calculations using either isolated or embedded clusters [37–39] and periodic models [36, 40], each method bearing its advantages and disadvantages. In particular, values obtained using small cluster models show significant variations with cluster size, reaching convergence only when systems containing more than 20 tetrahedral SiO_4 units are investigated [28]. In case of embedded clusters, for example within a QM-Pot approach, the influence of cluster size is much smaller although, as a downside, issues associated with embedding may arise. In this context, Brändle and Sauer reported that all the calculated DPE values for FAU and MFI are within a range 3 and 6 kJ mol^{-1} wide, respectively, while values for different crystalline structures span within a range of less than 30 kJ mol^{-1} [37, 41]. These findings would indicate that the intrinsic acidic strength of zeolites is hardly influenced by the framework structure. To avoid embedding artifacts, periodic DFT was used by Jones *et al.* [36] in a broad study of deprotonation energies for several zeolites, mapping every unique crystallographic position for the Al-Si substitution. They reported mean DPE values, obtained by averaging over the four distinct proton locations at each Al atom, in the range of 1201±11 kJ mol^{-1} for all crystalline frameworks considered. This investigation suggested that DPEs are insensitive to the Si−O−Al bond angles, but conversely exhibit a dependence on the framework densities [40, 42]. However, the employed method is not immune to errors, having to account for the artificial interactions arising among charged cells, created after the deprotonation of a zeolite site, in periodic calculations [43, 44]. More recently, the fact that the sites Brønsted acidity strength is inversely correlated with the framework density was confirmed by Trachta and coworkers

[45], which used a series of increasing-size cluster models to estimate the deprotonation energies in FAU, CHA, IFR, MOR, FER, MFI, and TON zeolites. After the results of cluster models have been corrected by applying an electrostatic embedding, from the proposed deprotonation energies reported there a mean value of 1245 ± 9 kJ mol^{-1} can be calculated, which is sensibly higher than the one obtained by Jones *et al.*

In spite of the significant number of studies reported on the topic, the effect of zeolite topology and composition on intrinsic acidity and reactivity is far from being fully understood. Many questions are still open and, especially from an atomistic-scale point of view, more accurate treatments are desirable, being however challenging the attempt to correlate computational results and experimental data, due to the inherent dissimilarity in what can be investigated in the two cases.

This work aims to add a piece of knowledge on the study of zeolite acidity based on quantum chemical descriptors, providing a comparative analysis of DPEs calculated through three different approaches, focusing on β-zeolite's framework (*BEA, if considering a mixture of polymorphs) as a case study.

Belonging to the large pore zeolites, BEA is one of the most notable and extensively used [46–51]. In BEA structure, silicon and oxygen atoms are linked to form 3D twelve-membered rings (diameter of 6-7 Å along the [010] and [100] axes, 5-6 Å along [001]), together with six, five and four-membered rings. This give rise to 9 and 17 crystallographically non-equivalent Si and O atoms, respectively, causing the topological possibility of 32 unique Brønsted acidic sites [zeo]. The intrinsic strength of all these sites is investigated in the present study by using i) an ONIOM method, ii) periodic DFT calculations and iii) a specially designed cluster approach based on the latter.

2. Models and Methods

2.1. ONIOM approach

From the periodic framework of the β-zeolite builded by using the crystallographic information file provided by International Zeolite Association (IZA) website [zeo], a portion of about 800 atoms was selected, featuring two intersections between the main twelve-membered ring channels (12T). To this fragment, terminal hydrogen atoms were added

4

to complete the valences of the dangling oxygen atoms, thus obtaining the model, consisting of 864 atoms, chosen as the real system for the subsequent ONIOM calculations (see Figure 1). Six model systems, in the following indicated as m1-m6, were selected, ranging in size from 39 to 102 atoms. Model systems from m1 to m4 were used to study more than one topological silicon, while the smallest ones, m5 and m6, were defined to investigate just one specific T site, namely T9 and T1, respectively, being these not properly embedded in the other models. In fact, careful attention has been paid so that the portion with the silicon atoms of interest was centered with respect to the model system itself, so to place these at a suitable distance in all directions from the boundary with the low level. Figure 2 shows the six model systems embedded in the real system and, in a close-up view of the model systems, all the labels of the investigated acidic sites.

Geometry optimizations were performed for: i) the silicalite systems as starting point, ii) the anionic structures with one Si atom replaced by one Al and iii) the neutral structures with aluminum and a hydrogen atom. In the latter, the hydrogen was positioned so that it interacted, in turn, with three of the four oxygen atoms of the AlO_4 tetrahedral unit. In the following the different acidic sites will be labeled as $TnOm$, where T is the tetrahedral center corresponding to the silicon atom substituted by aluminum whereas n and m are couples of numbers pointing out the specific topological site as reported in Figure 2. Excluding T5O14 and T6O14 sites, where the added hydrogen would not be accessible, 40 cases were obtained out of the 32 topologically distinct acidic sites of the β-zeolite. Some aluminum-hydrogen configurations were considered twice in different model systems, as an internal consistency check. The site-topological label assignment was made by comparison with labels reported in the crystallographic information file of the BEA framework, using the VESTA program [53].

[Figure 1 about here.]

[Figure 2 about here.]

Gaussian16 [54] was used with B3LYP hybrid exhange-correlation functional corrected by the third order Grimme empirical treatment of dispersion interactions (B3LYP-D3, [55]); the cc-pvdz basis set was employed for all atoms. The chosen low level of theory for the application of ONIOM was the Universal Force Field. A singlet multiplicity state

5

was considered for both high and low level. Inspection of the calculated harmonic vibrational normal modes confirmed that the investigated structures correspond to minima on the potential energy surface of their respective systems.

2.2. Periodic DFT calculations

The structural model used for periodic DFT calculations is the BEA unit cell (a = b = 12.631 Å, c = 26.186 Å, $\alpha = \beta = \gamma = 90°$) provided by IZA [zeo] and illustrated in Figure 3. Periodic geometry optimization were performed for the 30 structures originated by replacing, one at a time, all the topologically distinct silicon atoms with aluminum and adding one H atom on the corresponding not equivalent oxygen centers.

[Figure 3 about here.]

All periodic calculations were performed by using the SIESTA approach as implemented in the code [56] bearing the same name. The PBE exchange-correlation functional was chosen, along with double-ζ quality numerical basis sets generated with an energy shift of 0.005 Ry. New generation norm-conserving pseudopotentials were employed; they were taken from the database of the PseudoDojo project [57] (labeled as *nc-sr-04_pbe_standard*). The psml format is supported by the dedicated SIESTA-PSML-R1 version of the code [58]. Sampling was performed using a value of 450 Ry for the mesh cutoff and a 2×2×2 Monkhorst-Pack grid, which was refined at 4×4×4 after a first relaxation of the system geometry.

2.3. Cluster approach

Starting from optimized structures previously obtained through periodic DFT calculations, a zeolite unit cell reshaping procedure was performed to obtain clusters, then adjusted for the valences of terminal oxygen and silicon atoms. The reshape procedure, aimed at placing the acidic hydrogen atom roughly in the center of the new born fragment, replicates the neighborhood of the hydrogen atom which in the periodic calculation gave that specific arrangement after geometry optimization. Thus, the so obtained clusters are homogeneous, both each other and singly with their starting optimized structures. In detail, in order to build a reshaped cell, the position of the aluminum atom was fixed, both in the anionic and in the corresponding neutral structures, in the center of a new

defined cell, having the same a, b and c constants of the original BEA repetition unit. The atoms whose coordinates are inside this new cell do not undergo variations, while those that fall outside of it are translated back inside, by applying to them the a, b, c vectors. It should be noted that the choice of Al as the center of the new cell, being the interest in the definition of the clusters the acidic hydrogen atom, is justified by the proximity of the latter to Al and, on the other hand, its absence in the anionic structures. Figure 4 shows, taking the site T1O1 as an example, the system at the start and at the end of the described procedure, which was applied for the 30 neutral species and the 9 corresponding anions. After the reshaping stage is completed, we are left with many undersaturated Si and O nuclei at the cell boundaries. An automatic saturation procedure, whose algorithm is described in the following, was then applyed to prepare the structure for a cluster calculation. For every undersaturated nuclei in the cell, consider: case 1) it is a Si atom, so from 1 up to 3 neighboring oxygen atoms could be missing: in this case the correct number of hydrogen atoms were placed in an appropriate tetrahedral arrangement around Si, taking into account position and orientation of the already existing $Si-O$ bonds; whenever an $Si-H$ moiety was less than two $Si-O$ bonds apart from the acidic site, it was substituted by $Si-OH$; case 2) it is a O atom, in which case only a single neighboring Si could be missing, and consequently a single hydrogen was added at 109.5° $Si-O-H$ angle. It is worth to note that: i) in the authors' opinion, the average $Si-O-Si$ value of 136° typical of zeolites is too wide for a proper $Si-O-H$ angle, an issue that could give rise to energetic artifacts depending on the number of their occurrence, hence the choice for the 109.5° value; ii) all the terminating -OH groups are oriented in the same spatial direction (and so not in the direction of the next Si in the zeolite framework) in order to avoid the occurrence of having two saturating hydrogens too close each another, which is a possibility since two different oxygen atoms may be bonded to the same silicon atom. Wherever this is not the case and the saturated hydroxyl group is close to the Al region, the orientation was adjusted in order to match the one occurring in the zeolite structure. The final geometry was checked to ascertain that no border H-atom was less than 4.5 Å from the acid hydrogen site, a distance that was considered scarcely influent regarding the dispersion interactions between the real and the fictitious hydrogen atoms.

For the described cluster approach, the same exchange-correlation functional and basis set used for the model systems of the ONIOM calculations were employed. It should be emphasized that the SIESTA and the cluster approaches are intimately related one to the other and the latter, which starts from the optimized structures obtained by the periodic treatment, can be considered as an automatic, non-empirical correction of the former in view of the evaluation of deprotonation energies.

[Figure 4 about here.]

3. Results and Discussion

In Table 1, DPE values for the 30 investigated topologically distinct acidic sites of BEA, obtained by using the three chosen computational approaches (ONIOM, SIESTA, cluster) are reported as three different sets. Deprotonation energy was calculated merely as the difference between the SCF energy of the aluminated β-zeolite anionic form and the SCF energy of the corresponding neutral form. Extrapolated energies were used in the case of the ONIOM approach. Actually, the use of ONIOM allows to define systems small enough to make affordable the calculation of vibrational frequencies, hence thermochemical properties. By comparing the calculated DPE values based on the ONIOM energy with those based on the ONIOM enthalpy, it can be estimated that the thermal contributions to the deprotonation energy (leading to a decrease of the DPE) span between 27 and 36 kJ mol^{-1}, depending on the nature of the zeolite site. This range is in agreement with the average value of 29 kJ mol^{-1} estimated in the literature [45] for the contribution due to the difference of vibrational zero-point energies in various zeolites, and can be considered simply as a constant contribution as regards a discussion about the relative results obtained with the three approaches here described.

The three energy sets found with the different methods were normalized in the 0–100 interval following the expression

$$\text{DPN}_{\text{n},i}^{\text{M}} = 100 \cdot \frac{\text{DPE}_i^{\text{M}} - \text{DPE}_{\text{min}}^{\text{M}}}{\text{DPE}_{\text{max}}^{\text{M}} - \text{DPE}_{\text{min}}^{\text{M}}} \tag{1}$$

where the normalized deprotonation energy of the i-th site according to method M, $\text{DPN}_{\text{n},i}^{\text{M}}$, is defined with respect to the raw DPE_i^{M} and the minimum and maximum

DPE values found within the corresponding set. All the data were then collected in the histogram of Figure 5, which is divided into three equally spaced bands to qualitatively indicate low, medium and high site acidity, being clear that the x-axis is sorted in ascending order based on the numbering of silicon (and then oxygen) labels only.

A tentative explanation of the ONIOM behavior reported in the histogram is given in the following. As can be noticed from Figure 2, in β-zeolite the T8 and T9 sites feature only two non equivalent oxygen atoms (O11 and O16 the former, O3 and O15 the latter). The two T9O3 and the two T9O15 sites are well defined in the same m5 model. Further, as revealed by the presence of double ONIOM bars in the histograms reported in Figure 5, other cases have been examined twice (duplicate sites), using different model systems. This makes it possible to obtain indications on the suitability of the model system choice, thus of the application on this zeolitic system of the ONIOM method itself. Among the 8 duplicate sites there are some cases where the ONIOM results fall inside different acidity groups, depending on the involved model system. The most striking ones are precisely the sites T2O5 and T4O11, and, to a lesser extent, T2O7. As an example, T4O11 is predicted to have a very low acidity by the m1 model while is among the most acidic sites according to the m2 model. On the other hand, similar qualitative results are obtained in the case of T4O5 and T7O7 sites (belonging to the same acidity zone), while small differences are reported for T3O1, T3O8 and T7O8. Notably, in all the three duplicate sites exhibiting more significant differences the model system m1 is involved, always giving the highest value, which would suggest a bias of this model system. For the T4O5 site, instead, m1 and m2 are in excellent agreement, while T3O1 and T3O8 show only subtle differences between m1 and the other model systems in which they are taken into consideration. Without going into details on the many factors that are certainly involved, the phenomenon may find explanation in the basis nature of a model, which for definition cannot capture all facets of the reality. In fact, it is easy to imagine that the same ideal topological site of the periodic zeolite can be described differently by two different model systems. In particular, the neighborhood of the rings to which the site belongs can be different, being this neighborhood necessarily a subset of what defines the topology of the same model site.

[Table 1 about here.]

9

It is necessary to highlight that particular attention was given to ensure that the acidic hydrogen was surrounded by atoms treated at DFT level within the ONIOM approach, and that it was positioned at least 3 bonds away from the low-level region. However, in almost all the model systems the silicon atom which is replaced by the aluminum atom features only three of the four Si atoms belonging to the tetrahedrons around it in the high level of calculation. This could limit the relaxation of the structure during geometry optimization, with consequences on the deprotonation energies. Since this situation was also found in literature [29], it was tried to solve the problem by including the missing silicon and some other oxygen atoms in the model systems. This attempt anyway proved to be unviable due to the intrinsic characteristics of the β-zeolite structure. In fact the addition of atoms into the model system often makes ONIOM layers definition impossible, as an example showing one atom in the real system bonded to more than one atom of the model system. Even the shaping of smaller 5T systems centered at the topological silicon of interest was not always possible due to the same problems in the ONIOM partitioning. Li *et al.* in fact, got around the problem by removing some oxygen atoms from the high level, an expedient that created model systems which were not homogeneous with each other and that might cause significant artifacts considering their small size.

All this considered, the ONIOM approach does not seem a satisfactory mean to adequately investigate the acidity of the 9 topologically distinct site of the β-zeolite. In order to avoid the problem of both duplicate sites, differently described by the model systems, and of shaping incomplete silicon tetrahedron around the topological site, we suggest to eliminate the choice of model systems upstream, and carry out periodic calculations followed by a refining treatment using a cluster approach, as illustrated in the following.

Actually, a drawback still exists in using periodic DFT when dealing with charged unit cells, namely in geometry optimizations of zeolite anionic structures: the interaction between charges of all the images leads, in fact, to energy artifacts that must be taken into account and compensated. This is an open problem yet, as highlighted by the work of Iglesia *et al.* [36]. One of the best proposed procedures to address this issue contemplates an *a posteriori* correction, following the Freysoldt-Neugebauer-Van de Walle (FNV) scheme [43], which applies to the energies, while the respective geometries remain

10

unchanged. Therefore, one can reasonably trust on the optimized geometries found for anions and, as proposed in this work, use them as a starting point for a cluster DFT approach.

In such a method, each acidic site that in periodic calculations is located inside the unit cell, subject to periodic boundary conditions, is now described by a finite fragment of the zeolite framework. For this reason, changes to the starting structures are necessary to reproduce in the new system the chemical local environment that characterizes each site, hence the reshape procedure detailed in the Models and Methods section. The approach here proposed features several advantages: (i) it avoids issues arising in the choiche of a model system, (ii) even if the geometry optimization is not performed again, it is based on reliable geometries, properly adapted by placing the acidic hydrogen atom homogeneously in all the sites, (iii) without suffering from charges interaction artifacts, it supplies DPE values more accurate than those obtained by any periodic DFT analysis and (iv) it offers the possibility to choose exchange-correlation functionals and basis sets more appropriate, with respect to those commonly available in softwares for periodic calculations, to discriminate the intrinsic acidity of the zeolitic sites.

Referring to the DPE values obtained with the proposed cluster approach, an acidity strenght order of the investigated 30 topologically distinct acidic sites of BEA can be extrapolated. Among them 11 belongs to the middle portion of the range, 11 cases feature the highest instrinsic Brønsted acidity, in particular T7O7 and T8O11, and the remaining 8 sites are less acidic, especially T4O12, T1O2 and T6O12. In order to get a deeper insight into the cause of the acidity trend, a structural analysis of the 30 sites was performed in terms of the hydrogen bond parameters involving the acidic hydrogen atom. Structures with strong hydrogen bonds, namely those showing H-bond, O···H, distance ranging from 1.5 to 3.0 Å and O−H···O angle in-between 150° and 180° are depicted in Figure 6, in descending order of acidity. The presence of H-bonds was detected in almost all the sites belonging to the low and medium-low acidity groups and just occasionally in the other groups (high and medium-high acidity). When this last issue occurred, the site is less acid than the one which shares the same T and does not show H-bond formation, like it is the case, e.g., of T8O16 and T8O11. A correlation may be therefore drawn between hydrogen bond formation and the occurrence of a low acidity characterizing

11

the corresponding site. In particular, it has been devised that H-bonds are formed when proton donor and acceptor oxygen atoms belong to the same (5- or 6-membered) ring. At the bottom of the low acidity range, sites T4O12, T6O12 and T6O16 show two hydrogen bonds with the right orientation. The correlation above can be considered as a further evidence which substantiates the findings of Katada *et al.*[34] about the factors affecting the vibrational frequency of the O−H stretching, taken as an index of site acidity.

[Figure 6 about here.]

It is, at this point, noteworth to compare the most and the least acidic sites according to the three computational approaches employed. The site showing the highest intrinsic acidity is T8O11 according to the here proposed cluster approach (strictly followed by T7O7, the two sites showing the acidic hydrogen that protrude in the main channel, a fact surely auspicable when β-zeolite is to be used as an acidic catalyst), while T5O10 and T1O4 are indicated by ONIOM and SIESTA methods, respectively. In this respect, the ONIOM approach sensibly fails if compared to the cluster one.

The optimized ONIOM and SIESTA structures both show hydrogen bonds in the corresponding most acidic site (see Figure 6), being this occurrence the possible cause of their collocation within the medium acidity group when they are treated by the cluster approach. An excellent agreement between SIESTA and cluster is found regarding the least acidic site, as they both predict that this role belongs to the T4O12 site, where the proton is involved in two strong hydrogen bonds. Conversely, ONIOM indicates the near T4O9 site as the least acidic one, being in any case T4O12 in the region of the low acidity.

Deprotonation energies range from 1382 to 1275 kJ mol^{-1} in the case of ONIOM, while they are between 1049–1008 kJ mol^{-1} for periodic calculations and 1238–1179 kJ mol^{-1} employing the cluster approach. It must be noted that only the acidity interval resulting from this latter is in line with the one proposed for zeolites by Jones *et al.* [36] and Trachta *et al.* [35], while the one guessed by ONIOM is overestimated, probably due a destabilization of the anionic form caused by the fact that its negative charge cannot be properly delocalized on the small model systems. As a matter of fact, if the average of the Brønsted acidity of all the Al−O sites —evaluated by the cluster method— is

12

considered, the value of 1207 kJ mol^{-1}, with a root mean square deviation of 15 kJ mol^{-1}, is obtained.

A striking difference between the data of Jones *et al.* on β-zeolite and those obtained in this work is observed when the comparison between periodic and cluster outcomes is performed. Indeed, the DPE values reported by Jones *et al.* for BEA, according to their periodic calculations, are comprised between 1561 and 1583 kJ mol^{-1} (neglecting the Al5O14 and Al6O14 sites), and their ensemble averaged $\langle DPE \rangle$ decreases around 1200 kJ mol^{-1} only after applying an empirical shift determined by the comparison with previous results based on embedded or cluster models. Conversely, the periodic SIESTA results here reported, with an average DPE of 1025 kJ mol^{-1} (RMSD of 6 kJ mol^{-1}), are well below with respect to those of the cluster values. Still, Jones *et al.* [36] proved that their overestimated data were not due to simple problems related to the charged cell issue, since the FNV correction [43] just increased the divergence from the seemingly accepted value of 1200 kJ mol^{-1}. In fact, the FNV correction should destabilize the charged species and in any case, for singly negative charged systems and large employed cells, it should not have a utterly significant magnitude [59]. In the work of Trachta *et al.* [35] raw periodic data are not reported, but they get close to the mean value of 1245 kJ mol^{-1} after correction. Still, in one of the last works on zeolite acidity, specifically on the very same β-zeolite here investigated, Vorontsov and Smirniotis [60] reported indeed uncorrected data, according to which DPE values should be in the narrow 1592–1603 kJ mol^{-1} range. Since all the authors above used plane waves as basis set for their periodic calculations, it can be hypothesized that the divergence between ours and their data should be searched in the difference between the used computational approaches; in details, being the same the DFT exchange-correlation functional, it seems that a plane-wave type description of the zeolite electron density gives results which substantially differ from those obtained by a SIESTA-based approach using strictly localized numerical basis sets.

In order to better compare our results with those found in the literature and to report Brønsted acidities which depend only on the position of the Al/Si substituted T site, a Boltzmann average of the DPE values corresponding to different oxygen sites attached on the same T site was considered. Barrierless processes were assumed for the proton

shifts between the oxygen centers above. The energies used for the determination of Boltzmann populations are those obtained by means of the SIESTA approach for the optimized geometries (the relative energy values should be reliable, since they are those of neutral systems), while the DPE values employed in the average are those obtained with the cluster method (see Table 1). By taking a look at Table 2 it can be noticed that the ⟨DPE⟩ values span a narrower segment (45 kJ mol^{-1}) with respect to the raw values, showing a mean value of 1212.8 kJ mol^{-1}. Further, this acidity interval can be divided into three subranges, with an energy interval of ca. 10 kJ mol^{-1} in-between; in particular, the high acidity sites T7, T8 and 79 are in the 1195–1200 kJ mol^{-1} range, the medium acidity T1, T2, T3 and T5 sites are within 1209–1219 kJ mol^{-1} and the two low acidity sites T4 and T6 fall in the 1229–1238 kJ mol^{-1} range. If DPE differences within each interval are neglected, the following acidity ranking of the β-zeolite T sites can be finally written:

$$\text{T8} \approx \text{T7} \approx \text{T9} > \text{T5} \approx \text{T1} \approx \text{T3} \approx \text{T2} > \approx \text{T6} \approx \text{T4} \tag{2}$$

This ⟨DPE⟩ order is obviously affected by the stability of the protonated form, which in turn depends on the occurring of hydrogen bond interactions. If only the most acidic site of each TnOm set is considered for the ranking, this one would become

$$\text{T8} \approx \text{T7} > \text{T5} > \text{T4} \approx \text{T9} \approx \text{T1} > \text{T2} \approx \text{T3} > \text{T6} \tag{3}$$

with all the DPEs comprised in the 1179–1213 kJ mol^{-1} range. By comparing the two rankings above, the most striking difference is the position of T4, an issue which is not surprising since the most acid T4 site (T4O5) is also the least stable, being the very low acid T4O12 site the only one having an appreciable Boltzmann population at room temperature. Moreover, it is here to emphasize that the Boltzmann-averaged DPE ranking (2) could be somehow different if other computational approaches were employed; this not only for the approximations inherent in the modelistic choices but also for the intrinsic accuracy of energy differences calculated by (periodic) density functional theory, which could be pretty far from the chemical accuracy (4 kJ mol^{-1}) needed to obtain trustworthy Boltzmann populations. In particular, within the present investigated cases, we think that the position of T1 suffer from the largest uncertainty. As a matter of fact, T1 (and to a lesser extent T7) is the only site whose acidity is heavily affected by

the Boltzmann averaging procedure (see Table 2); the two sites T1O2 and T1O4 are essentially isoenergetic but their DPEs differ by ca. 35 kJ mol^{-1} according to the cluster approach (and also according to the SIESTA one, see Table 1): if the error on their energy difference was ± 4 kJ mol^{-1} (but almost surely it is much larger than this), the error on the $\langle$DPE$\rangle$ would be ± 12 kJ mol^{-1}, meaning that T1 would be tossed either high or low on the acidity scale.

Finally, the discrepancy between the position of T8 in the acidity order calculated by our cluster approach (guessing T8 as the most acidic site) and the one reported by Vorontsov and Smirniotis [60] (putting T8 as the least acidic) is to be discussed. In fact, the difference between the raw, periodic, DPE values of T8 and of the most acidic site (T2) according to Vorontsov and Smirniotis is only ca. 8 kJ mol^{-1}, and could be affected by accuracy flaws. The T8 site is indeed in the least acidic range if our SIESTA values are considered, but it becomes the one with the lowest DPE after the application of the cluster approach correction.

[Table 2 about here.]

4. Conclusions

The β-zeolite's Brønsted acidity has been characterized in terms of the deprotonation energy (DPE) values of 30 topologically distinct acidic sites. DPEs were computed through three different approaches within the DFT framework, namely: (i) an ONIOM embedding scheme, (ii) periodic calculations according to the SIESTA formalism and (iii) a novel cluster method specifically designed to avoid the disadvantages related to the other two approaches. By the cluster approach a range of nearly 60 kJ mol^{-1} was found which, divided into three equally spaced portions, gives 11, 11 and 8 sites setting high, medium and low Brønsted acidity, respectively. The formation of hydrogen bonds, actually detected in all the three groups of sites, was identified as a significant factor, if only to determine, within the same T site, to which oxygen atom the proton is preferentially bonded, hence site Boltzmann populations. As a matter of fact, if Boltzmann averaged DPE values are calculated, even considering that the limited accuracy of the computational methods could heavily influence the position of some sites in the acidity

15

scale, it can be concluded that three acidity groups invariably exist, which are separated by about 10 kJ mol^{-1} one from the other. This insight on the acidity of β-zeolite as well as the relative topology can provide fundamental information for the use of this material in catalysis, orienting the active sites optimization through the occurring relationship between the aluminum placement and the activity/selectivity of the catalyst.

A general disagreement is found between the results obtained by the employed approaches, ONIOM, SIESTA and cluster, both in the absolute and relative DPE values. If the cluster method is taken as the most appropriate, this disagreement is to be attributed to the difficulty in the definition of a generally reliable model system, in the case of ONIOM, and to the intrinsic problems of periodic formalisms related to charged cells, in the SIESTA case. Regarding the latter, it seems that the use of localized atomic orbitals, which defines the SIESTA formalism, leads to underestimate the site deprotonation energies in β-zeolite, oppositely to what happens in calculations based on plane waves, delocalized by definition. The suggested cluster approach, consisting in the evaluation of DPE by means of non-periodic single point DFT calculations starting from reshaped zeolite cell whose geometry was optimized by the SIESTA method, is therefore proposed as a suitable tool to correct in an algorithmic way the DPE values resulting from periodic calculations. This because it avoids the necessity of empirical corrections and constitutes a homogeneous computational model. Indeed, it would allow to treat essentially in the same modelistic way the zeolite acidic sites, possible modifiers of the acidity strength (like, *e.g.* defects or embedded metal particles) and the reactions in which zeolite catalitic activity is eventually involved. In the investigation of processes occurring inside the zeolite cavities, for example, the reacting molecule would conveniently result located at the center of the system, just like the zeolite proton itself. The simple cluster approach proposed in this work can be easily extended to other zeolite architectures without any conceptual modification.

Data Availability

Supporting materials is available. It contains the optimized geometries, in xyz format, of:

- the β-zeolite supercell used in the investigation;

16

- the ONIOM models m1-m6;

- the protonated form of all cluster models.

References

[1] Li, Y., Yu, J.. New stories of zeolite structures: their descriptions, determinations, predictions, and evaluations. Chem Rev 2014;114:7268–7316. doi:https://doi.org/10.1021/cr500010r.

[2] Dusselier, M., Davis, M.E.. Small-pore zeolites: Synthesis and catalysis. Chem Rev 2018;118:5265–5329. doi:https://doi.org/10.1021/acs.chemrev.7b00738.

[3] Tamizhdurai, P., Krishnan, P.S., Ramesh, A., Shanthi, K.. Isomerization of hydrocarbons over Pt supported on micro-mesoporous ZSM-5. Polyhedron 2018;154:314–324. doi: https://doi.org/10.1016/j.poly.2018.06.032.

[4] Berger, F., Rybicki, M., Sauer, J.. Adsorption and cracking of propane by zeolites of different pore size. J Catal 2021;395:117–128. doi:https://doi.org/10.1016/j.jcat.2020.12.008.

[5] Kaka Khel, T., Maki-Arvela, P., Azkaar, M., Vajglova, Z., Aho, A., Hemming, J., et al. Hexadecane hydrocracking for production of jet fuels from renewable diesel over proton and metal modified H-Beta zeolites. Mol Catal 2019;476:110515. doi:https://doi.org/10.1016/j.mcat.2019.110515.

[6] Wen, Z., Zhu, H., Zhu, X.. Density functional theory study of the zeolite-catalyzed methylation of benzene with methanol. Catal Lett 2020;150:21–30.

[7] Murzin, D.Yu.. Acid site density as a kinetic descriptor of catalytic reactions over zeolites. Chemistry 2022;4:1609–1623. doi:https://doi.org/10.3390/chemistry4040105.

[8] Sadovnikov, A.A., Arapova, O.V., Russo, V., Maximov, A.L., Murzin, D.Yu., Naranov, E.R.. Synergy of acidity and morphology of micro-/mesoporous materials in the solid-acid alkylation of toluene with 1-decene. Ind Eng Chem Res 2022;61:1994–2009. doi: https://doi.org/10.1021/acs.iecr.1c04169.

[9] Chizallet, C., bouchy, C., Larmier, K., Pirngruber, G.. Molecular views on mechanisms of brønsted acid-catalyzed reactions in zeolites. Chem Rev 2023;123:6107–6196. doi: https://doi.org/10.1021/acs.chemrev.2c00896.

[10] Liu, C., Li, G., Hensen, E.J.M., Pidko, E.A.. Relationship between acidity and catalytic reactivity of faujasite zeolite: A periodic DFT study. J Catal 2016;344:570–577. doi: https://doi.org/10.1016/j.jcat.2016.10.027.

[11] Vjunov, A., Fulton, J.L., Huthwelker, T., Pin, S., Mei, D., Schenter, G.K., et al. Quantitatively probing the Al distribution in zeolites. J Am Chem Soc 2014;136:8296–8306. doi: https://doi.org/10.1021/ja501361v.

[12] Zhai, D., Liu, Y., Zheng, H., Zhao, L., Gao, J., Xu, C., et al. A first-principles evaluation of the stability, accessibility, and strength of Brønsted acid sites in zeolites. J Catal 2017;352:627–637. doi:https://doi.org/10.1016/j.jcat.2017.06.035.

[13] Zhao, R., Zhao, Z., Li, S., Zhang, W.. Insights into the correlation of aluminum distribution

490 and Brønsted acidity in H-Beta zeolites from solid-state NMR spectroscopy and DFT calculations.
491 J Phys chem Lett 2017;8:2323–2327. doi:10.1021/acs.jpclett.7b00711.

[14] Arena, F., Ferrante, F., Di Chio, R., Bonura, G., Frusteri, F., Frusteri, L., et al. DFT and kinetic evidences of the preferential CO oxidation pattern of manganese dioxide catalysts in hydrogen stream (PROX). Appl Catal B: Env 2022;300:120715. doi: https://doi.org/10.1016/j.apcatb.2021.120715.

[15] Ferrante, F., Prestianni, A., Bertini, M., Duca, D.. H_2 transformations on graphene supported palladium cluster: DFT-MD simulations and NEB calculations. Catalysts 2020;10. doi: 10.3390/catal10111306.

[16] Ferrante, F., Nania, C., Duca, D.. Computational investigation of isoeugenol transformations on a platinum cluster – I: Direct deoxygenation to propylcyclohexane. Mol Catal 2022;529:112541. doi:https://doi.org/10.1016/j.mcat.2022.112541.

[17] Ferrante, F., Bertini, M., Ferlito, C., Lisuzzo, L., Lazzara, G., Duca, D.. A computational and experimental investigation of halloysite silicic surface modifications after alkaline treatment. Appl Clay Sci 2023;232:106813. doi:https://doi.org/10.1016/j.clay.2022.106813.

[18] Gueci, L., Ferrante, F., Prestianni, A., Di Chio, R., Patti, A.F., Duca, D., et al. DFT insights into the oxygen-assisted selective oxidation of benzyl alcohol on manganese dioxide catalysts. Inorg Chim Acta 2020;511:119812. doi:https://doi.org/10.1016/j.ica.2020.119812.

[19] Gueci, L., Ferrante, F., Prestianni, A., Arena, F., Duca, D.. Benzyl alcohol to benzaldehyde oxidation on MnO_x clusters: Unraveling atomistic features. Mol Catal 2021;513:111735. doi: https://doi.org/10.1016/j.mcat.2021.111735.

[20] Nania, C., Bertini, M., Gueci, L., Ferrante, F., Duca, D.. DFT insights into competing mechanisms of guaiacol hydrodeoxygenation on a platinum cluster. Phys Chem Chem Phys 2023;25:10460–10471. doi:https://doi.org/10.1039/D2CP06077A.

[21] Cortese, R., Campisi, D., Prestianni, A., Duca, D.. Alkane dehydrogenation on defective BN quasi-molecular nanoflakes: DFT studies. Mol Catal 2020;493:110891. doi: https://doi.org/10.1016/j.mcat.2020.110891.

[22] Gueci, L., Bertini, M., Nania, C., Ferrante, F., Duca, D.. DFT study of Pt particle growth inside β-zeolite cages. J Phys Chem C 2023;127:14765–14775. doi: https://doi.org/10.1021/acs.jpcc.3c02957.

[23] Broclawik, E., Kozyra, P., Mitoraj, M., Radon, M., Rejmak, P.. Zeolites at the molecular level: What can be learned from molecular modeling. Molecules 2021;26. doi:10.3390/molecules26061511.

[24] Ferrante, F., Rubino, T., Duca, D.. Butene isomerization and double-bond migration on the H-ZSM-5 outer surface: A density functional theory study. J Phys Chem C 2011;115:14862–14868. doi:https://doi.org/10.1021/jp203284f.

[25] Vorontsov, A.V., Valdes, H., Smirniotis, G.S.. Design of active sites in zeolite catalysts using modern semiempirical methods: The case of mordenite. Comput Theor Chem 2019;1166:112572. doi:https://doi.org/10.1016/j.comptc.2019.112572.

[26] Sandoval-Diaz, L.E., Gonzalez-Amaya, J.A., Trujillo, C.A.. General aspects of ze-

olite acidity characterization. Microporous Mesoporous Mater 2015;215:229–243. doi: https://doi.org/10.1016/j.micromeso.2015.04.038.

[27] Sazama, P., Tabor, E., Klein, P., Wichterlova, B., Sklenak, S., Mokrzycki, L., et al. Al-rich beta zeolites. Distribution of Al atoms in the framework and related protonic and metal-ion species. J Catal 2016;333:102–114. doi:https://doi.org/10.1016/j.jcat.2015.10.010.

[28] Boronat, M., Corma, A.. What is measured when measuring acidity in zeolites with probe molecules? ACS Catal 2019;9:1539–1548. doi:10.1021/acscatal.8b04317.

[29] Li, S., Zhao, Z., Zhao, R., Zhou, D., Zhang, W.. Aluminum location and acid strength in an aluminum-rich beta zeolite catalyst: A combined density functional theory and solid-state NMR study. ChemCatChem 2017;9:1494–1502. doi:https://doi.org/10.1002/cctc.201601623.

[30] Wang, S., He, Y., Jiao, W., Wang, J., Fan, W.. Recent experimental and theoretical studies on Al siting/acid site distribution in zeolite framework. Curr Opin Chem Eng 2019;23:146–154. doi:https://doi.org/10.1016/j.coche.2019.04.002.

[31] Niwa, M., Suzuki, K., Katada, N., Kanougi, T., Atoguchi, T.. Ammonia IRMS-TPD study on the distribution of acid sites in mordenite. J Phys Chem B 2005;109:18749–18757. doi: https://doi.org/10.1021/jp051304g.

[32] Suzuki, K., Katada, N., Niwa, M.. Detection and quantitative measurements of four kinds of OH in HY zeolite. J Phys Chem C 2007;111:894–900. doi:https://doi.org/10.1021/jp065054v.

[33] Suzuki, K., Sastre, G., Katada, N., Niwa, M.. Ammonia IRMS-TPD measurements and DFT calculation on acidic hydroxyl groups in CHA-type zeolites. Phys Chem Chem Phys 2007;9:5980–5987. doi:https://doi.org/10.1039/B711961E.

[34] Katada, N., Tamagawa, H., Niwa, M.. Quantitative analysis of acidic OH groups in zeolite by ammonia IRMS-TPD and DFT: Application to BEA. Catal Today 2014;226:37–46. doi: https://doi.org/10.1016/j.cattod.2013.08.006.

[35] Trachta, M., Bludský, O., Vakulík, J., Bulánek, R., Rubeš, M.. Investigation of brønsted acidity in zeolites through adsorbates with diverse proton affinities. Sci Rep 2023;13:12380. doi: https://doi.org/10.1021.

[36] Jones, A.J., Iglesia, E.. The strength of Brønsted acid sites in microporous aluminosilicates. ACS Catal 2015;5:5741–5755. doi:10.1021/acscatal.5b01133.

[37] Brändle, M., Sauer, J.. Acidity differences between inorganic solids induced by their framework structure. a combined quantum mechanics/molecular mechanics ab initio study on zeolites. J Am Chem, Soc, 1998;120:1556–1570. doi:https://doi.org/10.1021/ja9729037.

[38] Eichler, U., Brändle, M., Sauer, J.. Predicting absolute and site specific acidities for zeolite catalysts by a combined quantum mechanics/interatomic potential function approach. J Phys Chem B 1997;101:10035–10050. doi:https://doi.org/10.1021/jp971779a.

[39] Jones, A.J., Carr, R.T., Zones, S.I., Iglesia, E.. Acid strength and solvation in catalysis by MFI zeolites and effects of the identity, concentration and location of framework heteroatoms. J Catal 2014;312:58–68. doi:https://doi.org/10.1016/j.jcat.2014.01.007.

[40] Deshlahra, P., Iglesia, E.. Reactivity descriptors in acid catalysis: acid strength,

proton affinity and host–guest interactions. Chem Commun 2020;56:7371–7398. doi: https://doi.org/10.1039/D0CC02593C.

[41] Sauer, J., Sierka, M.. Combining quantum mechanics and interatomic potential functions in ab initio studies of extended systems. J Comput Chem 2000;21:1470–1493. doi: https://doi.org/10.1002/1096-987X(200012)21:16<1470::AID-JCC5>3.0.CO;2-L.

[42] Rybicki, M., Sauer, J.. Acid strength of zeolitic Brønsted sites - dependence on dielectric properties. Catal Today 2019;323:86–93. doi:https://doi.org/10.1016/j.cattod.2018.04.031.

[43] Freysoldt, C., Neugebauer, J., Van de Walle, C.G.. Fully ab initio finite-size corrections for charged-defect supercell calculations. Phys Rev Lett 2009;102:016402. doi: https://doi.org/10.1103/PhysRevLett.102.016402.

[44] Bruneval, F., Crocombette, J.P., Gonze, X., Dorado, B., Torrent, M., Jollet, F.. Consistent treatment of charged systems within periodic boundary conditions: The projector augmented-wave and pseudopotential methods revisited. Phys Rev B 2014;89:045116. doi: https://doi.org/10.1103/PhysRevB.89.045116.

[45] Trachta, M., Bulánek, R., Bludský, O., Rubeš, M.. Brønsted acidity in zeolites measured by deprotonation energy. Sci Rep 2022;12:7301. doi:https://doi.org/10.1038/s41598-022-11354-x.

[46] Boron, P., Rutkowska, M., Gil, B., Marszalek, B., Chmielarz, L., Dzwigaj, S.. Experimental evidence of the mechanism of selective catalytic reduction of NO with NH_3 over Fe-containing BEA zeolites. ChemSusChem 2019;12:692–705. doi:https://doi.org/10.1002/cssc.201801883.

[47] Gomes, G.J., Zalazar, M.F., Lindino, C.A., Scremin, F.R., Bittencourt, P.R.S., Costa, M.B., et al. Adsorption of acetic acid and methanol on H-beta zeolite: An experimental and theoretical study. Microporous Mesoporous Mater 2017;252:17–28. doi: https://doi.org/10.1016/j.micromeso.2017.06.008.

[48] Klinyod, S., Boekfa, B., Pornsatitworakul, S., Maihom, T., Jarussophon, N., Treesukol, P., et al. Theoretical and experimental study on the 7-hydroxy-4-methylcoumarin synthesis with H-Beta zeolite. ChemistrySelect 2019;4:10660–10667.

[49] Lei, Z., Liu, L., Dai, C.. Insight into the reaction mechanism and charge transfer analysis for the alkylation of benzene with propylene over H-beta zeolite. Mol Catal 2018;454:1–11. doi: https://doi.org/10.1016/j.mcat.2018.05.010.

[50] Mendes, P.S.F., Chizallet, C., Perez-Pellitero, J., Raybaud, P., Silva, J.M., Ribeiro, M.F., et al. Interplay of the adsorption of light and heavy paraffins in hydroisomerization over H-beta zeolite. Catal Sci Technol 2019;9:5368–5382. doi:https://doi.org/10.1039/C9CY00788A.

[51] Barakov, R., Shcherban, N., Maki-Arvela, P., Yaremov, P., Bezverkhyy, I., Warna, J., et al. Hierarchical beta zeolites as catalysts in α-pinene oxide isomerization. ACS Sustain Chem Eng 2022;10:6642–6656. doi:https://doi.org/10.1021/acssuschemeng.2c00441.

[zeo] Database of Zeolite Structures @ http://www.iza-structure.org/databases/. (accessed July 17, 2020); URL http://www.iza-structure.org/databases/.

[53] Momma, K., Izumi, F.. VESTA 3 for three-dimensional visualization of crystal, volumetric and morphology data. J Appl Crystallogr 2011;44:1272. doi:

607   https://doi.org/10.1107/S0021889811038970.

[54] Frisch, M.J., Trucks, G.W., Schlegel, H.B., Scuseria, G.E., Robb, M.A., Cheeseman, J.R., et al.
      Gaussian16 Revision C.01. 2016. Gaussian Inc. Wallingford CT.

[55] Grimme, S.. Supramolecular binding thermodynamics by dispersion-corrected density functional
      theory. Chem Eur J 2012;18:9955. doi:https://doi.org/10.1002/chem.201200497.

[56] Soler, J.M., Artacho, E., Gale, J.D., García, A., Junquera, J., Ordejón, P., et al. The SIESTA
      method for ab initio order-N materials simulation. J Phys Conden Matter 2002;14:2745–2779.
      doi:https://doi.org/10.1088/0953-8984/14/11/302.

[57] van Setten, M.J., Giantomassi, M., Bousquet, E., Verstraete, M.J., Hamann, D.R., Gonze, X.,
      et al. The PseudoDojo: Training and grading a 85 element optimized norm-conserving pseudopo-
      tential table. Comp Phys Commun 2018;226:39–54. doi:https://doi.org/10.1016/j.cpc.2018.01.012.

[58] Garcia, A., Verstraete, M.J., Pouillon, Y., Junquera, J.. The PSML format and library for norm-
      conserving pseudopotential data curation and interoperability. Comp Phys Commun 2018;227:51–
      71. doi:https://doi.org/10.1016/j.cpc.2018.02.011.

[59] Freysoldt, C., Neugebauer, J., Van de Walle, C.G.. Electrostatic interactions be-
      tween charged defects in supercells. Phys Status Solidi B 2011;248:1067–1076. doi:
      https://doi.org/10.1002/pssb.201046289.

[60] Vorontsov, A.V., Smirniotis, P.G.. DFT study on the stability and the acid
      strength of brønsted acid sites in zeolite β. J Phys Chem A 2022;126:7840–7851. doi:
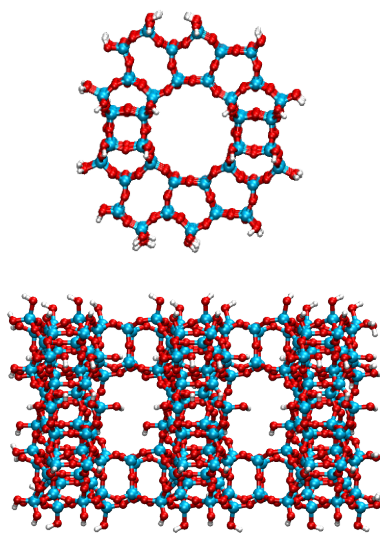   https://doi.org/10.1021/acs.jpca.2c04872.

21

List of Figures

22

Figure 1: Two views of the zeolite portion, consisting of 864 atoms, selected as the real system for the ONIOM approach (O=red, Si=cyan, H=white).
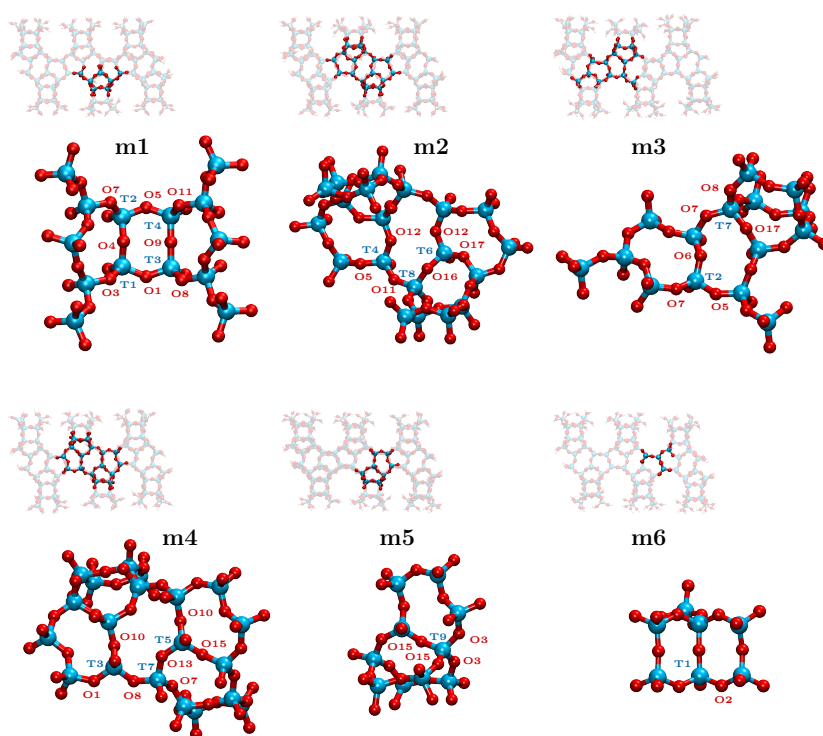
Figure 2: ONIOM model systems, m1-m6, embedded in the real system and, having chosen a convenient orientation, isolated. The topological labels of the examined tetrahedral and oxygen sites are reported for each model system.
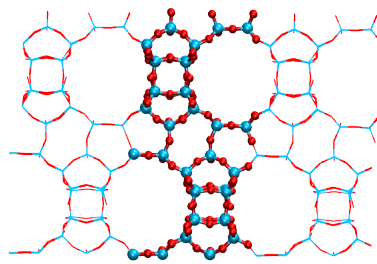
Figure 3: BEA unit cell of 192 atoms (ball-and-stick), within the periodic framework (wired), viewed along the ac plane. Cell parameters are: a = b = 12.631 Å, c = 26.186 Å, $\alpha = \beta = \gamma = 90°$.
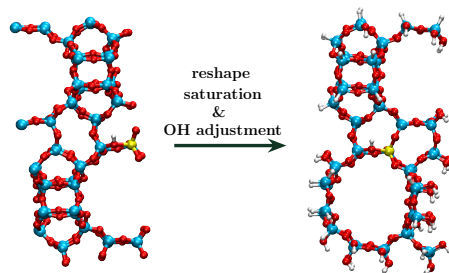
Figure 4: T1O1 acidic site within the BEA unit cell (left) and the fragment, with terminal hydrogen atoms, chosen to describe the same site (right) in the cluster approach. O=red, Si=cyan, Al=yellow, H=white.
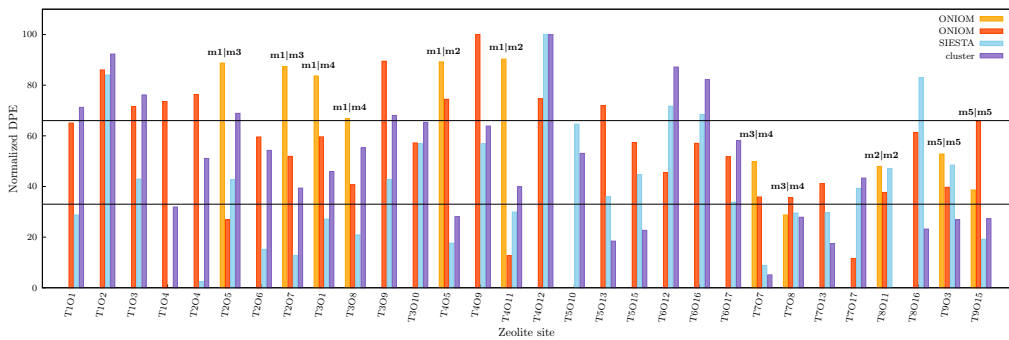
Figure 5: Sub-histograms of normalized DPE values calculated with ONIOM, SIESTA and cluster approaches characterizing the topologically distinct acidic sites of BEA. Whenever four bars are reported on a site sub-histogram, the first two refer to ONIOM results obtained from two different model systems (indicated by the labels above) or even from different sites of the same model system. A missing bar in a sub-histogram indicates the zero value for the corresponding case. Horizontal lines equally divide the histogram in three acidity zones.
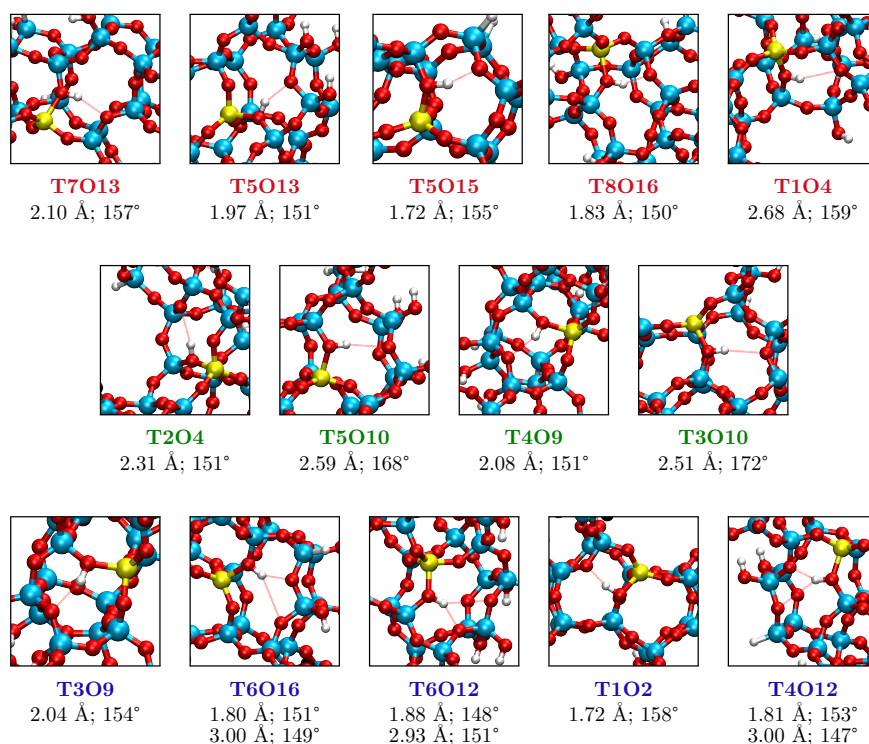
Figure 6: Structural details of the most significant hydrogen bonds detected in the topological configurations investigated, according to the cluster method. Below each image corresponding values of the O···H distances and O−H···O angles are reported. Different colors are used to label the acidity group to which each site belongs: high, medium and low acidity are associated with red, green and blue, respectively.

List of Tables

29

Table 1: DPE values[a] calculated whith the the ONIOM (O), SIESTA (S) and cluster (C) approaches.

site	O	S	C	site	O	S	C
T1O1	1344.9 (m1)[b]	1019.8	1220.9	**T4O12**	1355.2 (m2)	1049.3	1237.9
T1O2	1367.4 (m6)	1042.7	1233.3	**T5O10**	1275.3 (m4)	1034.7	1210.2
T1O3	1351.9 (m1)	1025.7	1223.8	**T5O13**	1352.3 (m4)	1022.8	1189.7
T1O4	1354.0 (m1)	1007.9	1197.6	**T5O15**	1336.6 (m4)	1026.4	1192.2
T2O4	1357.0 (m1)	1008.9	1209.0	**T6O12**	1324.0 (m2)	1037.6	1230.3
T2O5	1370.3 (m1) | 1304.0 (m3)	1025.6	1219.5	**T6O16**	1336.3 (m2)	1036.2	1227.4
T2O6	1339.0 (m3)	1014.2	1210.9	**T6O17**	1330.6 (m2)	1021.9	1213.2
T2O7	1368.7 (m1) | 1330.8 (m3)	1013.2	1202.1	**T7O7**	1328.6 (m3) | 1313.6 (m4)	1011.6	1181.8
T3O1	1364.8 (m1) | 1339.1 (m4)	1019.1	1205.9	**T7O8**	1306.1 (m3) | 1313.4 (m4)	1020.1	1195.3
T3O8	1346.8 (m1) | 1218.8 (m4)	1016.6	1211.5	**T7O13**	1319.3 (m4)	1020.2	1189.1
T3O9	1371.0 (m1)	1025.6	1219.0	**T7O17**	1287.6 (m3)	1024.2	1204.4
T3O10	1336.5 (m4)	1031.4	1217.4	**T8O11**	1326.6 (m2)	1027.4	1178.8
T4O5	1370.8 (m1) | 1355.0 (m2)	1015.2	1195.4	**T8O16**	1340.9 (m2)	1043.1	1192.5
T4O9	1382.3 (m1)	1031.4	1216.5	**T9O3**	1331.8 (m5) | 1318.1 (m5)	1028.0	1194.7
T4O11	1371.9 (m1) | 1288.8 (m2)	1020.3	1202.4	**T9O15**	1316.6 (m5) | 1345.8 (m5)	1015.8	1194.9

[a] Expressed in kJ mol^{-1}.
[b] The employed model system is indicated in parentheses.

Table 2: DPE values according to the Boltzmann average over the different oxygen sites next to a common tetrahedral site. The (e, p) numbers between parenthesis next to the O site are the energy (relative to the most stable case in the same T site) and population at room temperature, respectively.

T site	O sites	$\langle DPE \rangle^a$
1	O1 (23.0, 0.000); O2 (0.1, 0.487); O3 (17.1, 0.001); O4 (0.0, 0.512)	1215.0
2	O4 (16.7, 0.001); O5 (0.0, 0.982); O6 (11.4, 0.010); O7 (12.4, 0.007)	1219.3
3	O1 (12.3, 0.006); O8 (14.9, 0.002); O9 (5.8, 0.087); O10 (0.0, 0.905)	1217.5
4	O5 (34.1, 0.000); O9 (17.9, 0.001); O11 (29.0, 0.000); O12 (0.0, 0.999)	1237.9
5	O10 (0.0, 0.958); O13 (11.9, 0.008); O15 (8.3, 0.034)	1209.4
6	O12 (0.0, 0.632); O16 (1.3, 0.367); O17 (15.7, 0.001)	1229.2
7	O7 (12.6, 0.004); O8 (4.0, 0.140); O13 (4.0, 0.143); O17 (0.0, 0.712)	1199.6
8	O11 (14.8, 0.003); O16 (0.0, 0.997)	1192.5
9	O3 (0.0, 0.993); O15 (12.1, 0.007)	1194.7

^{a} Relative energy values and $\langle DPE \rangle$ are expressed in kJ mol^{-1}.